GPU-HADVPPM V1.0: A high-efficiency parallel GPU design of the piecewise parabolic method (PPM) for horizontal advection in an air quality model (CAMx V6.10)

Kai Cao[1], Qizhong Wu[1], Lingling Wang[2], Nan Wang[2], Huaqiong Cheng[1], Xiao Tang[3], Dongqing Li[1], and Lanning Wang[1]

[1]College of Global Change and Earth System Science, Beijing Normal University, Beijing 100875, China

[2]Henan Ecological Environment Monitoring and Safety Center, Henan Key Laboratory of Environmental Monitoring Technology, Zhengzhou 450000, China

[3]State Key Laboratory of Atmospheric Boundary Layer Physics and Atmospheric Chemistry, Institute of Atmospheric Physics, Chinese Academy of Science, Beijing 100029, China

Correspondence to: Qizhong Wu (wqizhong@bnu.edu.cn); Lingling Wang (928216422@qq.com); Lanning Wang (wangln@bnu.edu.cn)

Abstract. With semiconductor technology gradually approaching its physical and thermal limits, graphics processing units (GPUs) are becoming an attractive solution for many scientific applications due to their high performance. This paper presents an application of GPU accelerators in an air quality model. We demonstrate an approach that runs a PPM solver of horizontal advection (HADVPPM) for the air quality model CAMx on GPU clusters. Specifically, we first convert the HADVPPM to a new Compute Unified Device Architecture C (CUDA C) code to make it computable on the GPU (GPU-HADVPPM). Then, a series of optimization measures are taken, including reducing the CPU-GPU communication frequency, increasing the data size computation on the GPU, optimizing the GPU memory access and using thread and block indices to improve the overall computing performance of the CAMx model coupled with GPU-HADVPPM (named the CAMx-CUDA model). Finally, a heterogeneous, hybrid programming paradigm is presented and utilized with the GPU-HADVPPM on the GPU clusters with a message passing interface (MPI) and CUDA. The offline experimental results show that running GPU-HADVPPM on one NVIDIA Tesla K40m and an NVIDIA Tesla V100 GPU can achieve up to a 845.4x and 1113.6x

acceleration. By implementing a series of optimization schemes, the CAMx-CUDA model results in a 29.0x and 128.4x improvement in computational efficiency by using a GPU accelerator card on a K40m and V100 cluster, respectively. In terms of the single-module computational efficiency of GPU-HADVPPM, it can achieve 1.3x and 18.8x speedup on an NVIDIA Tesla K40m GPU and NVIDA Tesla V100 GPU, respectively. The multi-GPU acceleration algorithm enables a 4.5x speedup with 8 CPU cores and 8 GPU accelerators on a V100 cluster.

1. Introduction

Since the introduction of personal computers in the late 1980s, the computer and mobile device industry has created a flourishing worldwide market (Bleichrodt et al., 2012). In recent years, improvements of the central processing unit (CPU) performance have been limited by its heat dissipation, and the applicability of Moore's Law has flattened. A common trend in high-performance computing today is the utilization of hardware accelerators, which execute codes rich in data parallelism, to form high-performance heterogeneous systems. GPUs are widely used as accelerators due to their high peak performances. In the top ten supercomputing list released in December 2022 (https://www.top500.org/lists/top500/list/2022/11/, last access: 19 December 2022), there were seven heterogeneous supercomputing platforms built with CPU processors and GPU accelerators, of which the top one, Frontier at the Oak Ridge National Laboratory, uses AMD's third-generation EPYC CPU and AMD's Instinct MI250X GPU, and its computing performance reaches exascale levels (10^{18} calculations per second) for the first time (https://www.amd.com/en/press-releases/2022-05-30-world-s-first-exascale-supercomputer-powered-amd-epyc-processors-and-amd, last access: 19 December 2022). Such a powerful computing performance of the heterogeneous system not only injects new vitality into high-performance computing but also generates new solutions for improving the performance of geoscience numerical models.

The GPU has proven successful in weather models such as the nonhydrostatic icosahedral model (NIM; Govett et al., 2017), global/regional assimilation and prediction system (GRAPES; Xiao et al., 2022), weather research and forecasting model (WRF; Huang et al., 2011; Huang et al., 2012; Mielikainen et al., 2012a; Mielikainen et al., 2012b; Mielikainen et al., 2013a; Mielikainen et al., 2013b; Price et al., 2014; Huang et al., 2015), ocean models such as the LASG/IAP climate system ocean model (LICOM; Jiang et al., 2019; Wang et al., 2021a) and Princeton ocean model (POM; Xu et al., 2015) and earth system model of the Chinese Academy of Sciences (CAS-ESM; Wang et al., 2016; Wang et al., 2021b).

Govett et al. (2017) used open accelerator (OpenACC) directives to port the dynamics of NIM to the GPU and achieved a 2.5x acceleration. Additionally, using OpenACC directives, Xiao et al. (2022) ported the PRM (piecewise rational method) scalar advection scheme in GRAPES to the GPU, achieving up to 3.51x faster results than 32 CPU cores. In terms of the most widely used WRF, several parameterization schemes, such as the RRTMG_LW scheme (Price et al., 2014), 5-layer thermal diffusion scheme (Huang et al., 2015), Eta Ferrier cloud microphysics scheme (Huang et al., 2012), Goddard shortwave scheme (Mielikainen et al., 2012a), Kessler cloud microphysics scheme (Mielikainen et al., 2013b), SBU-YLIN scheme (Mielikainen et al., 2012b), WMS5 scheme (Huang et al., 2011) and WMS6 scheme (Mielikainen et al., 2013a), have been ported heterogeneously using CUDA C and achieved 37x~896x acceleration results. LICOM has conducted heterogeneous porting using OpenACC (Jiang et al., 2019) and used heterogeneous-compute interface for portability C (HIP C) technologies and achieved up to a 6.6x and 42x acceleration, respectively (Wang et al., 2021a). For the Princeton ocean model, Xu et al. (2015) use CUDA C to conduct heterogeneous porting and optimization, and the performance of gpu-POM v1.0 on four GPUs is comparable to that on the 408 standard Intel Xeon X5670 CPU cores. In terms of climate system models, Wang et al. (2016) and Wang et al. (2021b) used CUDA Fortran and CUDA C to conduct heterogeneous porting of the RRTMG_SW and RRTMG_LW schemes of the atmospheric component model of the CAS-ESM earth

89 system model and achieved a 38.88x and 77.78x acceleration, respectively.

90 Programming a GPU accelerator can be a difficult and error-prone process that

91 requires specially designed programming methods. There are three widely used

92 methods for porting programs to GPUs, as described above. The first method uses the

93 OpenACC directive (https://www.openacc.org/, last access: 19 December 2022), which

94 provides a set of high-level directives that enable C/C++ and Fortran programmers to

95 utilize accelerators. The second method uses CUDA Fortran. CUDA Fortran is a

96 software compiler that was codeveloped by the Portland Group (PGI) and NVIDIA,

97 and is a tool chain for building performance-optimized GPU-accelerated Fortran

98 applications targeting the NVIDIA GPU platform (https://developer.nvidia.com/cuda-

99 fortran, last access: 19 December 2022). Using CUDA C involves rewriting the entire

100 program using the standard C programming language and low-level CUDA subroutines

101 (https://developer.nvidia.com/cuda-toolkit, last access: 19 December 2022) to support

102 the NVIDIA GPU accelerator. Compared to the other two technologies, the CUDA C

103 porting scheme is the most complex but it has the highest computational performance

104 (Mielikainen et al., 2012b; Wahib and Maruyama, 2013; Xu et al., 2015).

105 Air quality models are critical for understanding how the chemistry and

106 composition of the atmosphere may change throughout the 21st century, as well as for

107 preparing adaptive responses or developing mitigation strategies. Because air quality

108 models need to take into account the complex physicochemical processes that occur in

109 the atmosphere of anthropogenic and natural emissions, simulations are

110 computationally expensive. Compared to other geoscientific numerical models, few

111 studies have conducted a heterogeneous porting of air quality models. In this study, the

112 CUDA C scheme, implemented in this paper, conducted a hotspot module porting of

113 CAMx to improve the computation efficiency.

2. The CAMx model and experiments

2.1. Model description

The CAMx model is a state-of-the air quality model developed by Ramboll Environ (https://www.camx.com/, last access: 19 December 2022). CAMx version 6.10 (CAMx V6.10; ENVIRON, 2014) is chosen in this study; it simulates the emission, dispersion, chemical reaction and removal of pollutants by marching the Eulerian continuity equation forward in time for each chemical species on a system of nested three-dimensional grids. The Eulerian continuity equation is expressed mathematically in terrain-following height coordinates as Formula (1):

$$\frac{\partial c_i}{\partial t} = -\nabla_H \cdot V_H c_i + \left[\frac{\partial (c_i \eta)}{\partial z} - c_i \frac{\partial^2 h}{\partial z \partial t} \right] + \nabla \cdot \rho K \nabla (c_i / \rho)$$

$$+ \left. \frac{\partial c_i}{\partial t} \right|_{Emission} + \left. \frac{\partial c_i}{\partial t} \right|_{Chemistry} + \left. \frac{\partial c_i}{\partial t} \right|_{Removal} \tag{1}$$

$$\nabla_H \cdot \rho V_H = \frac{m^2}{A_{yz}} \frac{\partial}{\partial x} \left(\frac{u A_{yz} \rho}{m} \right) + \frac{m^2}{A_{xz}} \frac{\partial}{\partial y} \left(\frac{v A_{xz} \rho}{m} \right) \tag{2}$$

The first term on the right-hand side represents horizontal advection. In numerical methods, the horizontal advection equation (described in Formula (2)) is performed using the area preserving flux-form advection solver of the piecewise parabolic method (PPM) of Colella and Woodward (1984) as implemented by Odman and Ingram (1996). The PPM horizontal advection solution (HADVPPM) was incorporated into the CAMx model because it provides higher order accuracy with minimal numerical diffusion.

In the Fortran code implementation of the HADVPPM scheme, the CAMx main program calls the emistrns program, which mainly performs physical processes such as emission, diffusion, advection and dry/wet deposition of pollutants. Then, the horizontal advection program is invoked by the emistrns program to solve the horizontal advection equation by using the HADVPPM scheme.

2.2. Benchmark performance experiments

The first porting step is to test the performance of the CAMx benchmark version and identify the model's hotspots. On the Intel x86 CPU platform, we launch two processes concurrently to run the CAMx, and take advantage of the Intel trace analyser collector (ITAC; https://www.intel.com/content/www/us/en/docs/trace-analyzer-collector/get-started-guide/2021-4/overview.html, last access: 19 December 2022) and the Intel VTune profiler (VTune;https://www.intel.com/content/www/us/en/develop/documentation/vtune-help/top.html, last access: 19 December 2022) performance analysis tools to collect performance information during the CAMx operation.

The general MPI performance can be reported by the ITAC tool, and MPI load balance information, computation and communication profiling of each process is shown in Fig. 1a. During the running process of the CAMx model, Process 0 (P0) spends 99.6% of the time on the MPI_Barrier function and only 0.4% of the time on computation, while Process 1 (P1) spends 99.8% of its time computation and only 0.2% of its time receiving messages from P0. It is apparent that the parallel design of the CAMx model adopts the Master-Slave mode, and P0 is responsible for inputting and outputting the data and calling the MPI_Barrier function to synchronize the process, so there is a lot of MPI waiting time. The other processes are responsible for computation.

The VTune tool detects each module's runtime and the most time-consuming functions on P1. As shown in Figure 1b, the top four time-consuming modules are chemistry, diffusion, horizontal advection and vertical advection in the CAMx model. In the above four modules, the top five most time-consuming programs are the ebirate, hadvppm, tridiag, diffus and ebisolv programs, and the total runtime of P1 is 325.1 seconds. Top1 and Top2's most time-consuming programs take 49.4 and 35.6 seconds, respectively.

By consideration, the hadvppm program was selected to conduct heterogeneous porting for several reasons. First, the advection module is one of the air quality model's compulsory modules, and is mainly used to simulate the transport process of air

pollutants, additionally it is also a hotspot module detected by the Intel VTune tool. The typical air quality models, CAMx, CMAQ and NAQPMS, include advection modules and use the exact PPM advection solver. The heterogeneous version developed in this study can be directly applied to the above models. Furthermore, the weather model (e.g., WRF) also contains an advection module, so this study's heterogeneous porting method and experience can be used for reference. Therefore, a GPU acceleration version of the HADVPPM scheme, namely, GPU-HADVPPM, is built to improve the CAMx performance.
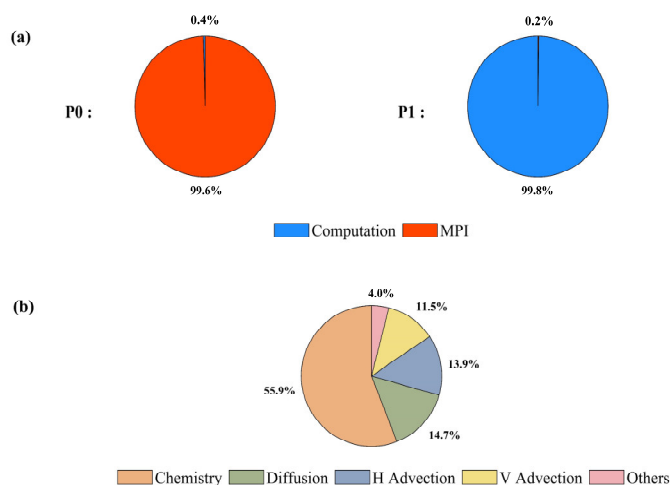
Figure 1. The computation performance of the modules in the CAMx model. (a) Computation and communication profiling of P0 and P1. (b) Overhead proportions of P1. The top four most time-consuming modules are chemistry, diffusion, horizontal advection and vertical advection.

2.3. Porting scheme introduction

The CAMx-CUDA heterogeneous scheme is shown in Figure 2. The second time-consuming hadvppm program in the CAMx model was selected to implement heterogeneous porting. To map the hadvppm program to the GPU, the Fortran code was converted to standard C code. Then, the CUDA programming language, which was tailor-made for NVIDIA, was added to convert the standard C code into CUDA C for

185 data-parallel execution on the GPU, as GPU-HADVPPM. It prepared the input data for

186 GPU-HADVPPM by constructing random numbers, and tested its offline performance

187 on the GPU platform.

188   After coupling the GPU-HADVPPM to the CAMx model, the advection module

189 code was optimized according to the characteristics of the GPU architecture to improve

190 the overall computational efficiency on the CPU-GPU heterogeneous platform. Then,

191 the multi-CPU core and multi-GPU card acceleration algorithm was adopted to improve

192 the parallel extensibility of heterogeneous computing. Finally, the coupling

193 performance test is implemented after verifying the different CAMx model simulation

194 results.
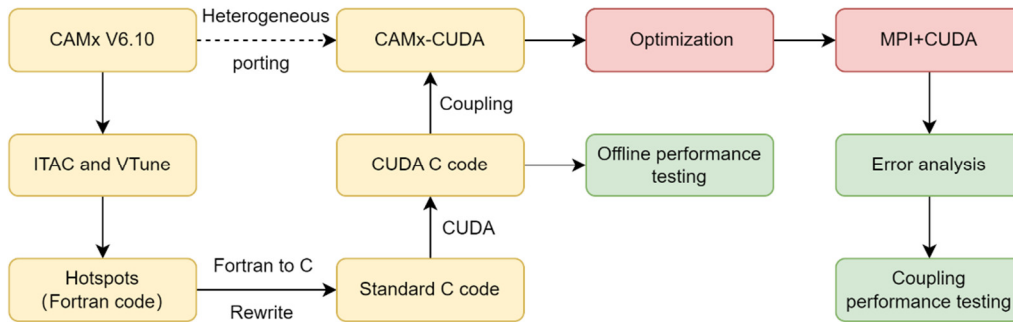
195

196 **Figure 2.** Heterogeneous porting scheme of the CAMx-CUDA model.

197 **2.4.   Hardware components and software environment of the testing system**

198   The experiments are conducted on two GPU clusters, K40m and V100. The

199 hardware components and software environment of the two clusters are listed in Table

200 1. The K40m cluster is equipped with two 2.5 GHz 16-core Intel Xeon E5-2682 v4

201 CPU processors and one NVIDIA Tesla K40m GPU card on each node. The NVIDIA

202 Tesla K40m GPU has 2880 CUDA cores with 12 GB of memory. The V100 cluster

203 contains two 2.7 GHz 24-core Intel Xeon Platinum 8168 processors and eight NVIDIA

204 Tesla V100 GPU cards with 5120 CUDA cores and 16 GB memory on each card.

205 **Table 1.** Configurations of GPU cluster.

Hardware components	
CPU	**GPU**

	Intel Xeon E5-2682 v4 CPU @2.5 GHz, 16 cores	NVIDIA Tesla K40m, 2880 CUDA cores, 12GB memory
K40m cluster		
V100 cluster	Intel Xeon Platinum 8168 CPU @2.7 GHz, 24 cores	NVIDIA Tesla V100, 5120 CUDA cores, 16GB memory
	Software environment	
	Compiler and MPI	**Programming Model**
K40m cluster	Intel-2021.4.0	CUDA-10.2
V100 cluster	Intel-2019.1.144	CUDA-10.0

206   For Fortran and standard C programming, Intel Toolkit (including compiler and

207 MPI library) version 2021.4.0 and version 2019.1.144 are employed for compiling on

208 an Intel Xeon E4-2682 v4 CPU and Intel Xeon Platinum 8168 CPU, respectively. Then,

209 CUDA version 10.2 and version 10.0 are employed on an NVIDIA Tesla K40m GPU

210 and NVIDIA Tesla V100 GPU. CUDA (NVIDIA, 2020) is an extension of the C

211 programming language that offers direct programming of the GPUs. In CUDA

212 programming, a kernel is actually a subroutine that can be executed on the GPU. The

213 underlying code in the kernel is divided into a series of threads, each with a unique "ID"

214 number that simultaneously process different data through a single-instruction multiple-

215 thread (SIMT) parallel mode. These threads are grouped into equal-sized thread blocks,

216 which are organized into a grid.

217 **3.   Porting and optimization of the CAMx advection module on a heterogeneous**

218   **platform**

219 **3.1.   Mapping the HADVPPM scheme to the GPU**

220 **3.1.1.   Manual code translation from Fortran to standard C**

221   As the CAMx V6.10 code was written in Fortran 90, we rewrote the hadvppm

222 program from Fortran to CUDA C. As an intermediate conversion step, we refactor the

223 original Fortran code using standard C. During the refactoring, some of the

224 considerations are listed in Table 2:

225   (1) The subroutine name refactored with standard C must be followed by an

226 underscore identifier, which can only be recognized when Fortran calls.

227   (2) In the Fortran language, the parameters are transferred by a memory address

228 by default. In the case of mixed programming in Fortran and standard C, the parameters

229 transferred by Fortran are processed by the pointer in standard C.

230   (3) Variable precision types defined in standard C must be strictly consistent with

231 those in Fortran.

232   (4) Some built-in functions in Fortran are not available in standard C, and need to

233 be defined in the standard C macro definitions.

234   (5) For multidimensional arrays, Fortran and standard C follow a column-major

235 and row-major order, and in-memory read and write, respectively;

236   (6) Array subscripts in Fortran and standard C are indexed from any integer and 0,

237 respectively.

238 **Table 2.** Some considerations during Fortran to C refactoring.

	Fortran code	**C code**
Function name	*subroutine hadvppm()*	*void hadvppm()*
Parameter passing	*hadvppm(nn, dt,dx, con,vel, area,areav, flxarr,mynn)*	*hadvppm(int *nn, float *dt, float *dx, float *con, float *vel, float *area, float *areav, float *flxarr, int *mynn)*
Variable precision	*real(kind=8) x*	*double x*
Built-in functions	*max*	*#define Max(a, b) ((a)>(b)?(a):(b))*
Memory read and write for multidimensional array	Column-major	Row-major
Array subscript index	Starting from any integer	Starting from 0

239

3.1.2. Converting standard C code into CUDA C

241   After refactoring the Fortran code of the hadvppm program with standard C,

242 CUDA was used to convert the C code into CUDA C to make it computable on the
243 GPU. A standard C program using CUDA extensions distributes a large number of
244 copies of the kernel functions into available multiprocessors and executes them
245 simultaneously on the GPU.

246   Figure 3 shows the GPU-HADVPPM implementation process. As mentioned in
247 Sect. 2.1, the xyadvec program calls the hadvppm program to solve the horizontal
248 advection function. Since the rewritten CUDA program cannot be called directly by the
249 Fortran program (xyadvec.f), we add an intermediate subroutine (hadvppm.c) as an
250 interface to transfer the parameters and data required for GPU computing from the
251 xyadvec Fortran program to the hadvppm_kernel CUDA C program.

252   A CUDA program automatically uses numerous threads on the GPU to execute
253 kernel functions. Therefore, the hadvppm_kernel CUDA C program first calculates the
254 number of parallel threads according to the array dimension. Then, the GPU memory
255 is allocated, and the parameters and data are copied from the CPU to the GPU. As the
256 CUDA program launches a large number of parallel threads to execute kernel functions
257 simultaneously, the computation results will be copied from the GPU back to the CPU.
258 Finally, the GPU memory is released, and the data computed on the GPU are returned
259 to the xyadvec program via the hadvppm C program.
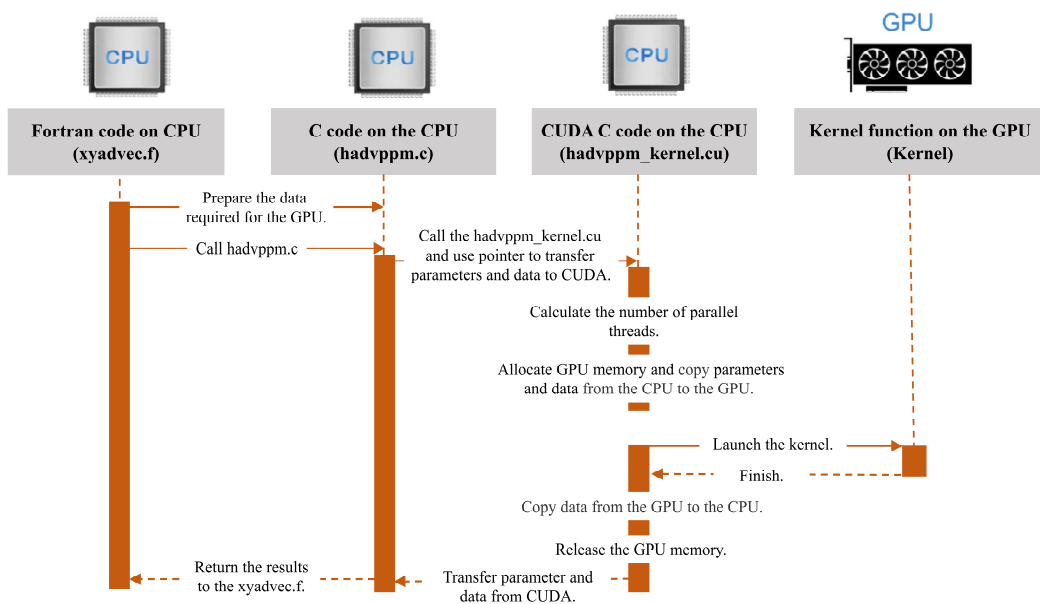
260

261 **Figure 3.** The calling and computation process of the GPU-HADVPPM on the CPU-GPU

262   heterogeneous platform.

3.2.   Coupling and optimization of the GPU-HADVPPM scheme on a single GPU

264   After the hadvppm program was rewritten with standard C and CUDA, the

265   implementation process of the HADVPPM scheme was loaded from the CPU to the

266   GPU. Then, we coupled the GPU-HADVPPM to the CAMx model. For ease of

267   description, we will refer to this original heterogeneous version of CAMx as CAMx-

268   CUDA V1.0. In CAMx-CUDA V1.0, four external loops are nested when the hadvppm

269   C program is called by the xyadvec program. This will result in widespread data

270   transfers from the CPU to the GPU over the PCIe bus within a time step, making the

271   computation of CAMx-CUDA V1.0 inefficient.

272   Therefore, we optimize the xyadvec Fortran program to significantly reduce the

273   frequency of data transmission between the CPU and GPU, increase the amount of data

274   computation on the GPU, and improve the total computing efficiency of the CAMx on

275   the CPU-GPU heterogeneous platforms. In the original CAMx-CUDA V1.0, four

276   external loops outside the hadvppm C program, and several one-dimensional arrays, are

277   computed before calling the hadvppm C program. Then, the CPU will frequently launch

278   the GPU and transfer data to it within a time step. When the code optimization is

279   completed, the three- or four-dimensional arrays required for a GPU computation

280   within a time step will be sorted before calling the hadvppm C program, and then the

281   CPU will package and transfer the arrays to the GPU in batches. An example of the

282   xyadvec Fortran program optimization is shown in Figure S1.

283   The details of the four different versions are shown in Table 3. In CAMx-CUDA

284   V1.0, the Fortran code of the HADVPPM scheme was rewritten using standard C and

285   CUDA, and the xyadvec program was not optimized. The dimensions of the c1d

286   variable array transmitted to the GPU in the X and Y directions are 157 and 145 in this

287   case, respectively. In CAMx-CUDA V1.1 and CAMx-CUDA V1.2, the c1d variable

288   transmitted from the CPU to GPU is expanded to two (approximately 23,000 numbers)

289   and four dimensions (approximately 27.4 million numbers) by optimizing the xyadvec

290   Fortran program and hadvppm_kernel CUDA C program, respectively.

291   The order in which the data are accessed in GPU memory affects the

292 computational efficiency of the code. In CAMx-CUDA V1.3 of Table 4, we further

293 optimized the order in which the data are accessed in GPU memory based on the order

294 in which they are stored in memory and eliminated the unnecessary assignment loops

295 that were added due to the difference in memory read order between Fortran and C.

296   As described in Sect. 2.4, a thread is the basic unit of parallelism in CUDA

297 programming. The thread structure is organized into a three-level hierarchy. The highest

298 level is a grid, which consists of three-dimensional thread blocks. The second level is a

299 block, which also consists of three-dimensional threads. The built-in CUDA variable

300 *threadIdx.x* determines a unique thread "ID" number inside a thread block. Similarly,

301 the built-in variables *blockIdx.x* and *blockIdx.y* determine which block to execute on,

302 and the size of the block is determined by using the built-in variable *blockdim.x*. For

303 the two-dimensional horizontal grid points, many threads and blocks can be organized

304 so that each CUDA thread computes the results for different spatial positions

305 simultaneously.

306   Before CAMx-CUDA V1.4, the loops for the three-dimensional spatial grid points

307 (i,j,k) are replaced by index computations using only the thread index ($i = threadIdx.x$

308 $+ blockIdx.x*blockDim.x$) to use the thread indices to simultaneously compute the grid

309 point in the x or y direction. To take full advantage of the thousands of threads in the

310 GPU, we implement thread and block indices ($i = threadIdx.x + blockIdx.x*blockDim.x;$

311 $j = blockIdx.y$) to simultaneously compute all the horizontal grid points (*i,j*) in CAMx-

312 CUDA V1.4. This is permitted because there are no interactions among the horizontal

313 grid points.

314 **Table 3.** The details of different CAMx-CUDA versions during optimization.

Version	Major revisions	Amount of data computation on GPU
CAMx-CUDA V1.0	The Fortran code of the HADVPPM subroutine was rewritten using standard C and CUDA, and *xyadvec.f* was not optimized.	157 and 145 in the x direction and y direction for the c1d variable, respectively.
CAMx-CUDA V1.1	Optimize *xyadec.f* and	157×145,

	hadvppm_kernel.cu to expand the dimension of the array transmitted to the GPU from 1-dimensional to 2-dimensional.	approximately 23,000 numbers for the c2d variable.
CAMx-CUDA V1.2	Based on the CAMx-CUDA V1.1, the dimension of the array transmitted to the GPU is extended from 2 to 4 dimensions.	157×145×14×86, approximately 27.4 million numbers for the c4d variable.
CAMx-CUDA V1.3	Based on the CAMx-CUDA V1.2, the order of GPU memory access is optimized and unnecessary assignment loops are eliminated.	157×145×14×86, approximately 27.4 million numbers for the c4d variable.
CAMx-CUDA V1.4	Based on the CAMx-CUDA V1.3, using thread and block indices ($i = threadIdx.x + blockIdx.x*blockDim.x; j = blockIdx.y$).	157×145×14×86, approximately 27.4 million numbers for the c4d variable.

3.3. MPI+CUDA acceleration algorithm of CAMx-CUDA on multiple GPUs

Generally, superlarge clusters have thousands of compute nodes. The current CAMx V6.10, implemented by adopting MPI communication technology, typically runs on dozens of compute nodes. Once the GPU-HADVPPM is coupled into the CAMx, it also has to run on multiple compute nodes that are equipped with one or more GPUs on each node. To make full use of multicore and multi-GPU supercomputers, and further improve the overall computational performance of CAMx-CUDA, we adopt a parallel architecture with an MPI+CUDA hybrid paradigm; that is, the collaborative computing strategy of multiple CPU cores and multiple GPU cards is adopted during the operation of the CAMx-CUDA model. Adopting this strategy, the GPU-HADVPPM can run on multiple GPUs, and the Fortran code of the other modules in the CAMx-CUDA model can run on multiple CPU cores.

As shown in Figure 4, after the simulated region is subdivided by MPI, a CPU core is responsible for the computation of a subregion. To improve the total computational performance of the CAMx-CUDA model, we further used the NVIDIA CUDA library to obtain the number of GPUs per node and then used the MPI process ID and remainder function to determine the GPU ID to be launched by each node.

333 Finally, we used the NVIDIA CUDA library, cudaSetDevice, to configure a GPU card

334 for each CPU core.

335 According to the benchmark performance experiments, the parallel design of

336 CAMx adopts the master-slave mode, and P0 is responsible for inputting and outputting

337 data. If two processes (P0 and P1) were launched, only the P1 and its configured GPU

338 participate in integration.
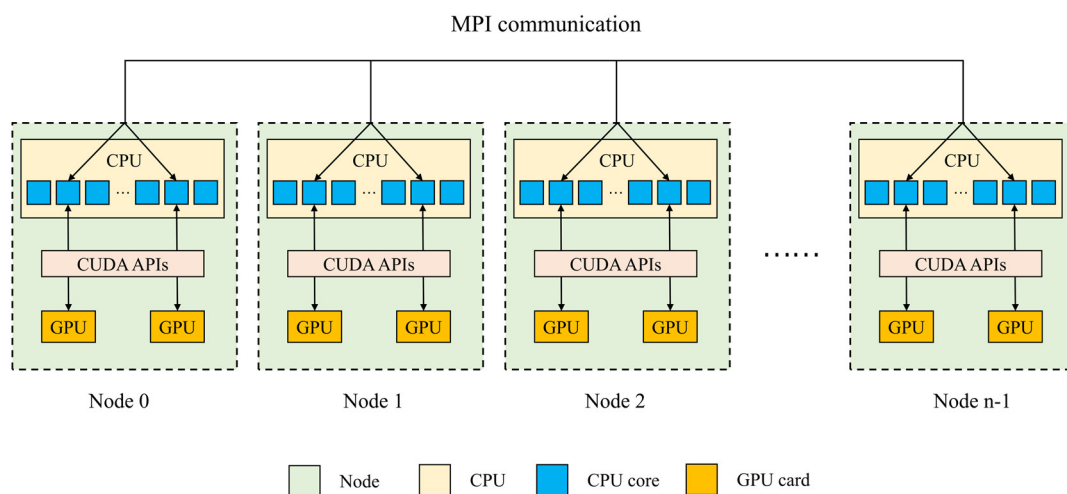
339

340 **Figure 4.** An example of parallel architecture with an MPI+CUDA hybrid paradigm on multiple

341 GPUs.

4. Experimental results

343 The validation and evaluation of porting the HADVPPM scheme from the CPU to

344 the GPU platform were conducted using offline and coupling performance experiments.

345 First, we validated the results between the different CAMx versions, and then the offline

346 performance of the GPU-HADVPPM on a single GPU was tested by offline

347 experiments. Finally, coupling performance experiments illustrate its potential in three

348 dimensions with varying chemical regimes. In Sect.4.2 and Sect.4.4, the CAMx

349 versions of the HADVPPM scheme written in Fortran, standard C and CUDA C are

350 named F, C and CUDA C, respectively.

 4.1. Experimental setup

352   The test case is a 48 h simulation covering Beijing, Tianjin and part of the Hebei

353 Province region. The horizontal resolution is 3 km with 145×157 grid boxes. The

354 model adopted 14 vertical layers. The simulation started at 12:00 UTC on 01 November

355 2020 and ended at 12:00 UTC on 03 November 2020. The meteorological fields driving

356 the CAMx model were provided by the weather research and forecasting (WRF;

357 Skamarock et al., 2008) model. The sparse matrix operator kernel emission (SMOKE;

358 Houyoux and Vukovich, 1999) version 2.4 model is used to provide gridded emission

359 data for the CAMx model. The emission inventories (Sun et al., 2022) include the

360 regional emissions in East Asia that were obtained from the transport and chemical

361 evolution over the Pacific (TRACE-P; Streets et al., 2003; Streets et al., 2006) project,

362 30-min (approximately 55.6 km at mid-latitude) spatial resolution Intercontinental

363 chemical transport experiment-Phase B (INTEX-B; Zhang et al., 2009) and the updated

364 regional emission inventories in North China. The physical and chemical numerical

365 methods selected during the CAMx model integration are listed in Table S2.

366   **4.2. Error analysis**

367   The hourly concentrations of different CAMx simulations (Fortran, C, and CUDA

368 C versions) are compared to verify the usefulness of the CUDA C version of CAMx for

369 numerical precision for scientific usage. Here, we chose six major species, i.e., SO_2, O_3,

370 NO_2, CO, H_2O_2 and PSO_4, after 48 h of integration to verify the results. Due to the

371 differences in programming languages and hardware, the simulation results are affected

372 during the porting process. Figures 5~7 present the spatial distributions of SO_2, O_3, NO_2,

373 CO, H_2O_2 and PSO_4, as well as the absolute errors (AEs) of their concentrations from

374 different CAMx versions. The species' spatial patterns of the three CAMx versions are

375 visually very similar. Between the Fortran and C versions, especially, the AEs in all the

376 grid boxes are in the range of ±0.01 ppbV (the unit of PSO_4 is $\mu g \cdot m^{-3}$). During the

377 porting process, the primary error comes from converting standard C to CUDA C, and

378 the main reason is related to the hardware difference between the CPU and GPU. Due

379 to the slight difference in data operation and accuracy between the CPU and GPU

380 (NVIDIA,2023), the concentration variable of the hadvppm program appears to have

381 minimal negative values (approximately $-10^{-9} \sim -10^{-4}$) when integrated on the GPU.

382 To allow the program to continue running, we forcibly replace these negative values

383 with 10^{-9}. It is because these negative values are replaced by positive values that the

384 simulation results are biased. In general, for SO_2, O_3, NO_2, H_2O_2 and PSO_4, the AEs in

385 the majority of the grid boxes are in the range of ± 0.8 ppbV or $\mu g \cdot m^{-3}$ between the

386 standard C and CUDA C versions; for CO, because its background concentration is

387 higher, the AEs of the standard C and CUDA C versions are outside that range, and fall

388 into the range of -8 and 8 ppbV in some grid boxes and shows more obvious AEs than

389 the other species.
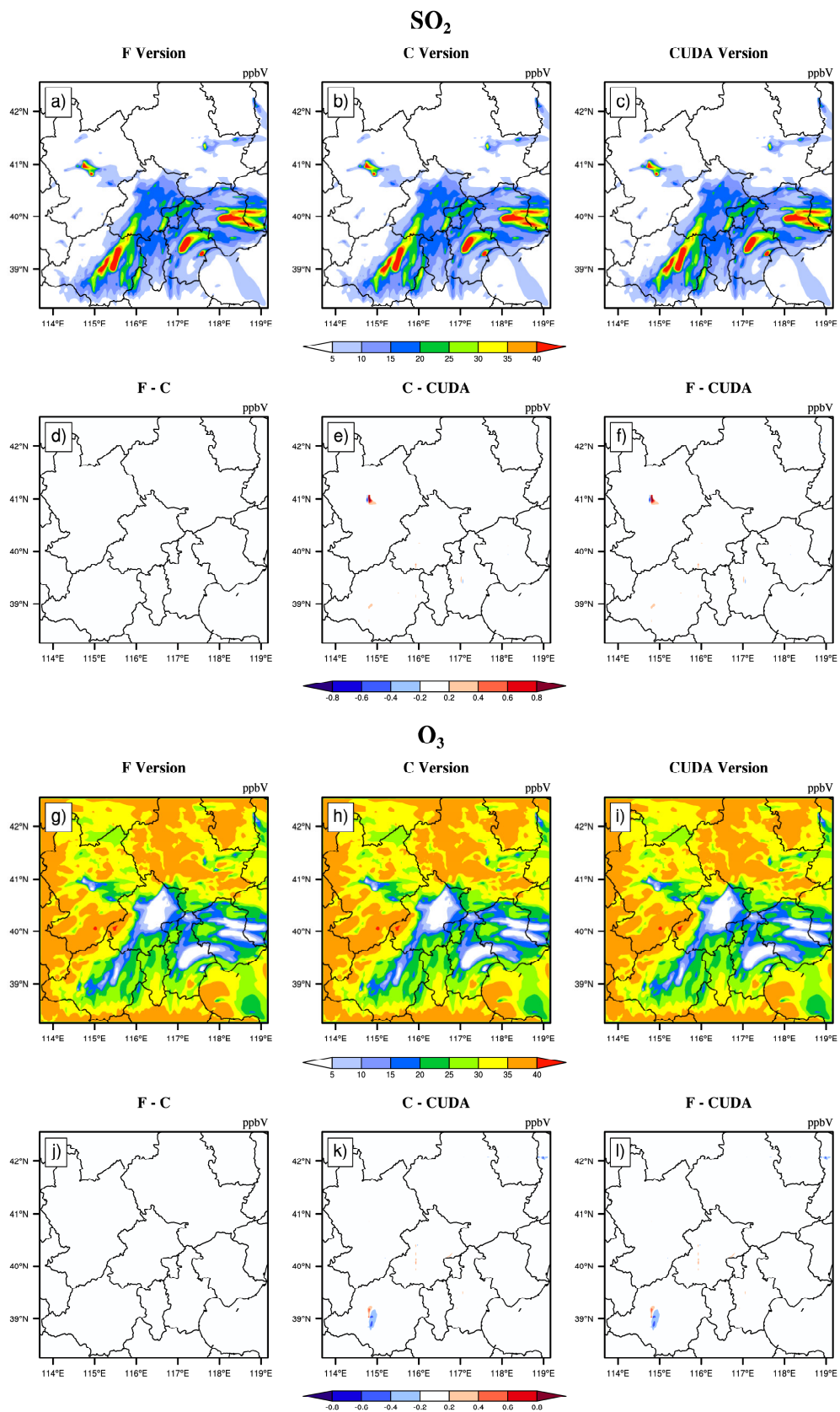
Figure 5. SO$_2$ and O$_3$ concentrations outputted by the CAMx model for the Fortran, standard C, and

392 CUDA C versions. Panels (a) and (g) are from the Fortran versions. Panels (b) and (h) are from the

393 standard C versions. Panels (c) and (i) are from the CUDA C versions. Panels (d) and (j) are the

394 output concentration differences of the Fortran and standard C versions. Panels (e) and (k) are the

395 output concentration differences of the standard C and CUDA C versions. Panels (f) and (l) are the

396 output concentration differences of the Fortran and CUDA C versions.
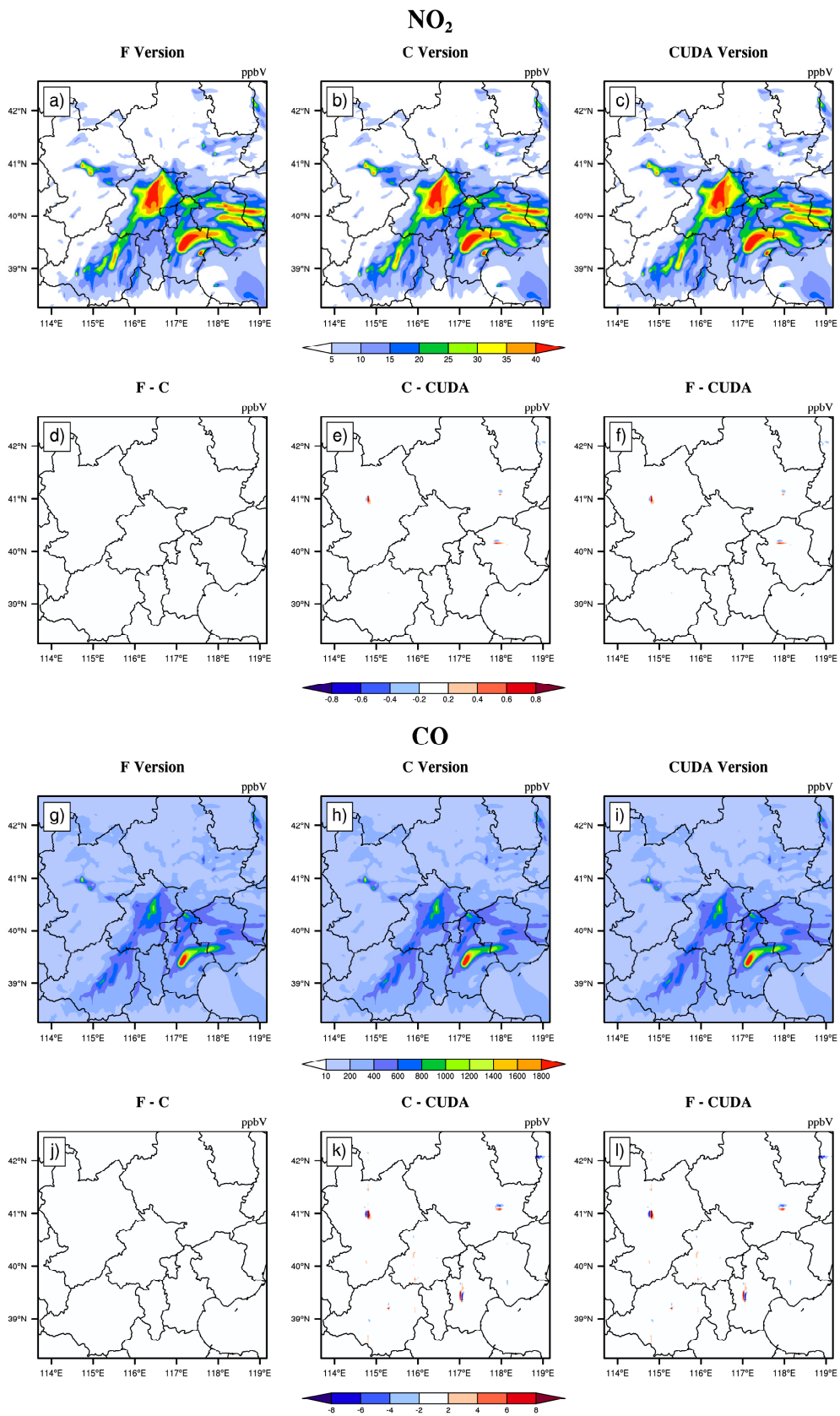
398 **Figure 6.** NO₂ and CO concentrations outputted by the CAMx model for the Fortran, standard C,

399 and CUDA C versions. Panels (a) and (g) are from the Fortran versions. Panels (b) and (h) are from

400 the standard C versions. Panels (c) and (i) are from the CUDA C versions. Panels (d) and (j) are the

401 output concentration differences of the Fortran and standard C versions. Panels (e) and (k) are the

402 output concentration differences of the standard C and CUDA C versions. Panels (f) and (l) are the

403 output concentration differences of the Fortran and CUDA C versions.
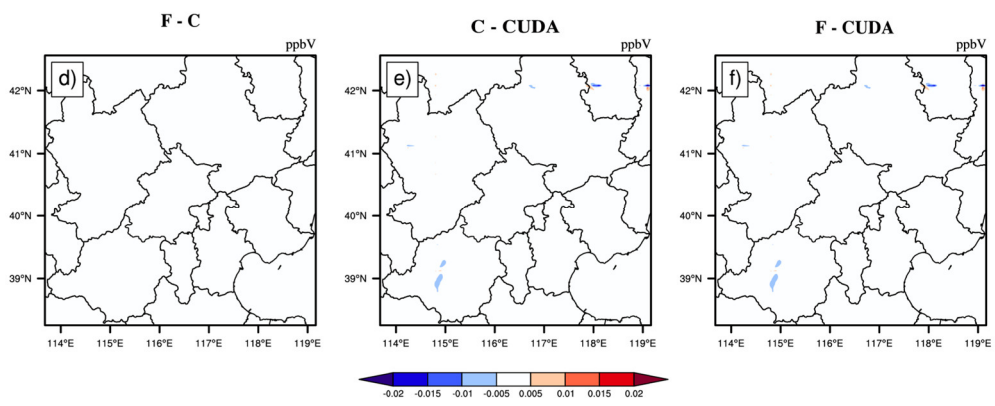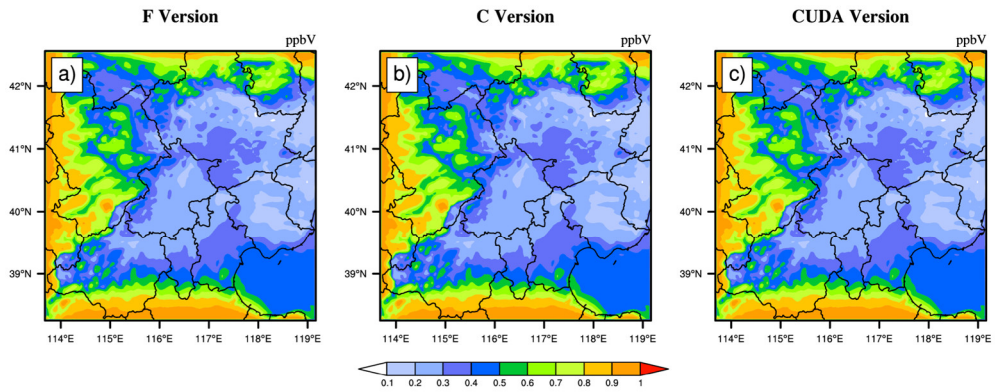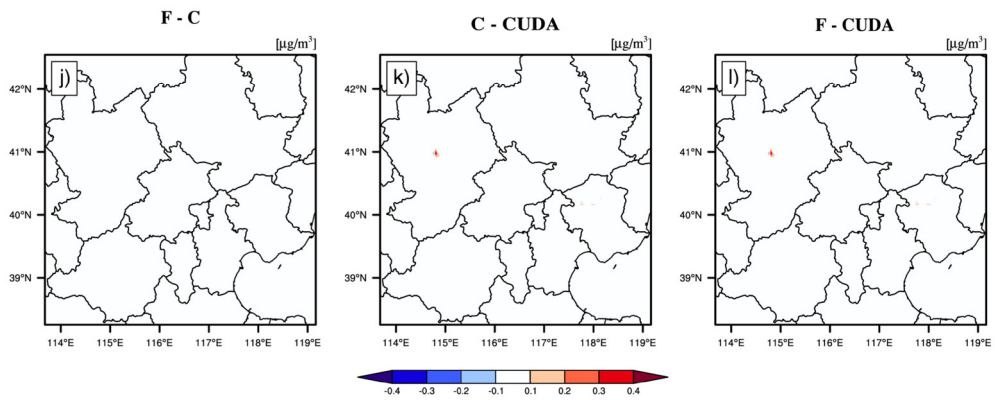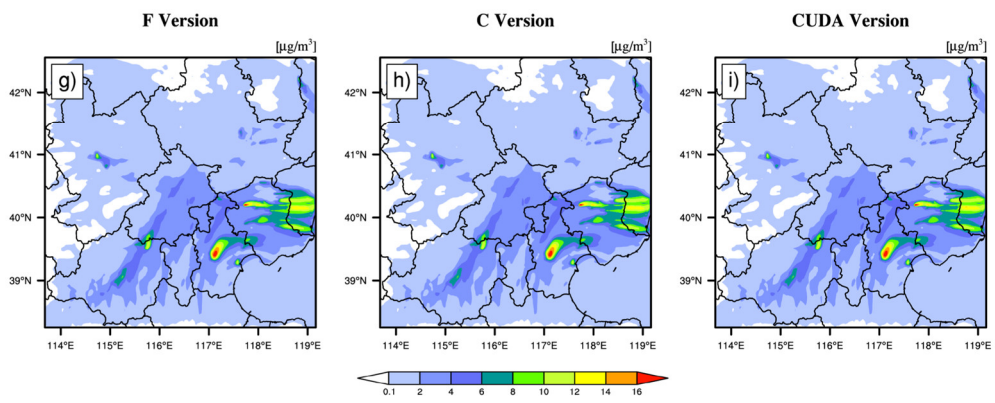
Figure 7. H_2O_2 and PSO_4 concentrations output by the CAMx model for the Fortran, standard C, and CUDA C versions. Panels (a) and (g) are from the Fortran versions. Panels (b) and (h) are from the standard C versions. Panels (c) and (i) are from the CUDA C versions. Panels (d) and (j) are the output concentration differences of Fortran and standard C versions. Panels (e) and (k) are the output concentration differences of the standard C and CUDA C versions. Panels (f) and (l) are the output concentration differences of the Fortran and CUDA C versions.

Figure 8 shows the boxplot of the AEs and relative error (REs) in all the grid boxes for the six species during the porting process. As described above, the AEs and REs introduced by Fortran to the standard C code refactoring process are significantly small, and the primary error comes from converting standard C to CUDA C. Statistically, the average AEs (REs) of SO_2, O_3, NO_2, CO, H_2O_2 and PSO_4 were -0.0009 ppbV (-0.01%), 0.0004 ppbV (-0.004%), 0.0005 ppbV (0.008%), 0.03 ppbV (0.01%), 2.1×10^{-5} ppbV (-0.01%) and 0.0002 $\mu g \cdot m^{-3}$ (0.0023%), respectively, between the Fortran and CUDA C versions. In terms of the time series, the regionally averaged time series of the three versions are almost consistent (as shown in Figure S2), and the maximum AEs for the above six species are 0.001 ppbv, 0.005 ppbv, 0.002 ppbv, 0.03 ppbv, 0.0001 ppbv and 0.0002 $\mu g \cdot m^{-3}$, respectively, between the Fortran and CUDA C versions.
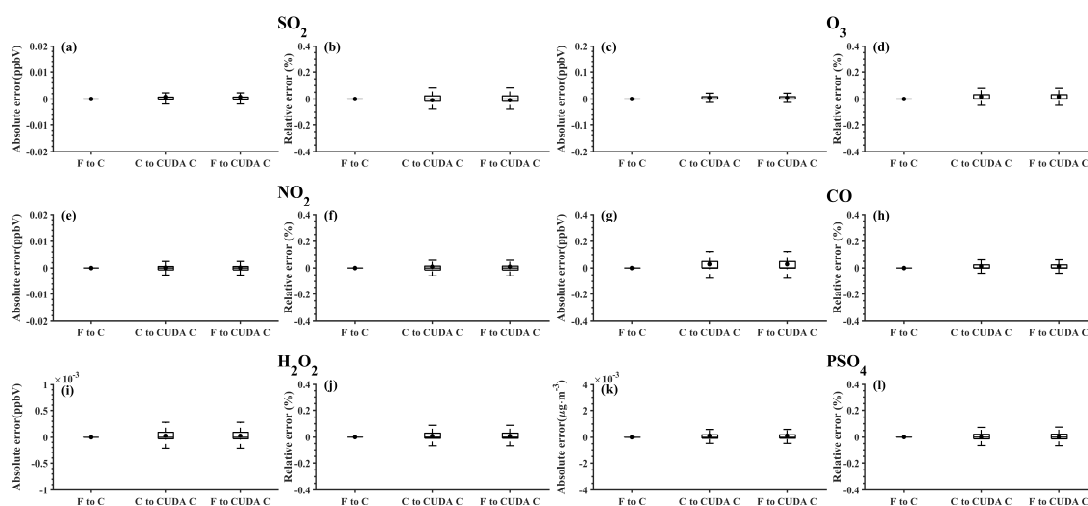
Figure 8. The distributions of absolute errors and relative errors for SO_2, O_3, NO_2, CO, H_2O_2 and PSO_4 in all of the grid boxes after 48 hours of integration.

Figure 9 presents the regionally averaged time series and the AEs of SO_2, O_3, NO_2, CO, H_2O_2 and PSO_4. The time series between the different versions is almost consistent,

427 and the maximum AEs for the above six species are 0.001 ppbv, 0.005 ppbv, 0.002 ppbv,

428 0.03 ppbv, 0.0001 ppbv and 0.0002 $\mu g \cdot m^{-3}$, respectively, between the Fortran and

429 CUDA C versions.

430 It is difficult to verify the scientific applicability of the results from the CUDA C

431 version because the programming language and hardware are different between the

432 Fortran and CUDA C versions. Here, we used the evaluation method of Wang et al.

433 (2021a) to compute the root mean square errors (RMSEs) of SO_2, O_3, NO_2, CO, H_2O_2

434 and PSO_4 between the Fortran and CUDA C versions, which are 0.0007 ppbV, 0.001

435 ppbV, 0.0002 ppbV, 0.0005 ppbV, 0.00003 ppbV and 0.0004 $\mu g \cdot m^{-3}$, respectively,

436 much smaller than the spatial variation of the whole region, which is 7.0 ppbV

437 (approximately 0.004%), 9.7 ppbV (approximately 0.003%), 7.4 ppbV (approximately

438 0.003%), 142.2 ppbV (approximately 0.006%), 0.2 ppbv (approximately 0.015%) and

439 1.7 $\mu g \cdot m^{-3}$ (approximately 0.004%). The bias between CUDA C and the Fortran

440 version of the above six species is negligible compared with their own spatial changes,

441 and the results of the CUDA C version are generally acceptable for research purposes.

442

4.3. Offline performance comparison of GPU-HADVPPM

444 As described in Sect. 4.2, we validate that the CAMx model result of the CUDA

445 C version is generally acceptable for scientific research. We tested the offline

446 performance of the HADVPPM and GPU-HADVPPM schemes on 1 CPU core and 1

447 GPU card. There are 7 variables input into the HADVPPM program, which are nn, dt,

448 dx, con, vel, area and areav, and their specific meanings are shown in Table S1.

449 First, we use the random_number function in Fortran to create random single-

450 precision floating-point numbers of different sizes for the above 7 variables, and then

451 transmit these random numbers to the hadvppm Fortran program and hadvppm_kernel

452 CUDA C program for computation. Finally, we test the offline performance of the

453 HADVPPM and GPU-HADVPPM on the CPU and GPU platforms. During the offline

454 performance experiments, we used two different CPUs and GPUs described in Sect.

455 2.4., and the experimental results are shown in Figure 9.

On the CPU platform, the wall time of the hadvppm Fortran program does not change significantly when the data size is less than 1000. With the increase in the data size, its wall time increases linearly. When the data size reaches 10^7, the wall time of the hadvppm Fortran program on the Intel Xeon E5-2682v4 and Intel Platinum 8168 CPU platforms is 1737.3 ms and 1319.0 ms, respectively. On the GPU platform, the reconstructed and extended CUDA C program implements parallel computation of multiple grid points by executing a large number of kernel function copies, so the computational efficiency of the hadvppm_kernel CUDA C code on it is significantly improved. In the size of 10^7 random numbers, the hadvppm_kernel CUDA C program takes only 12.1 ms and 1.6 ms to complete the computation on the NVIDIA Tesla K40m and NVIDIA Tesla V100 GPU.

Figure 9. (b) shows the speedup of HADVPPM and GPU-HADVPPM on the CPU platform and GPU platform under different data sizes. When mapping the HADVPPM scheme to the GPU, the computational efficiency under different data sizes is not only significantly improved, but the larger the data size is, the more obvious the acceleration effect of the GPU-HADVPPM. For example, in the size of 10^7 random numbers, the GPU-HADVPPM achieved a 1113.6x and 845.4x acceleration on the NVIDIA Tesla V100 GPU, respectively, compared to the two CPU platforms. Although the K40m GPU's single-card computing performance is slightly lower than that of the V100 GPU, GPU-HADVPPM can also achieve up to a 143.3x and 108.8x acceleration.

As described in Sect. 3.2, the thread is the most basic GPU unit for parallel computing. Each dimension of the three-dimensional block can contain a maximum number of threads of 1024, 1024 and 64. Each dimension of the three-dimensional grid can contain a maximum number of blocks of $2^{31} - 1$, 65535, and 65535. It is theoretically possible to distribute a large number of copies of kernel functions into tens of billions of threads for parallel computing without exceeding the GPU memory. In the offline performance experiments, the GPU achieved up to 10 million threads of parallel computing, while the CPU can only use serial cyclic computation. Therefore, GPU-HADVPPM achieves a maximum acceleration of approximately 1100x without

485 I/O. In addition to this study, the GPU-based SBU-YLIN scheme in the WRF model

486 can achieve a 896x acceleration compared to the Fortran implementation running on

487 the CPU (Mielikainen et al., 2012b).
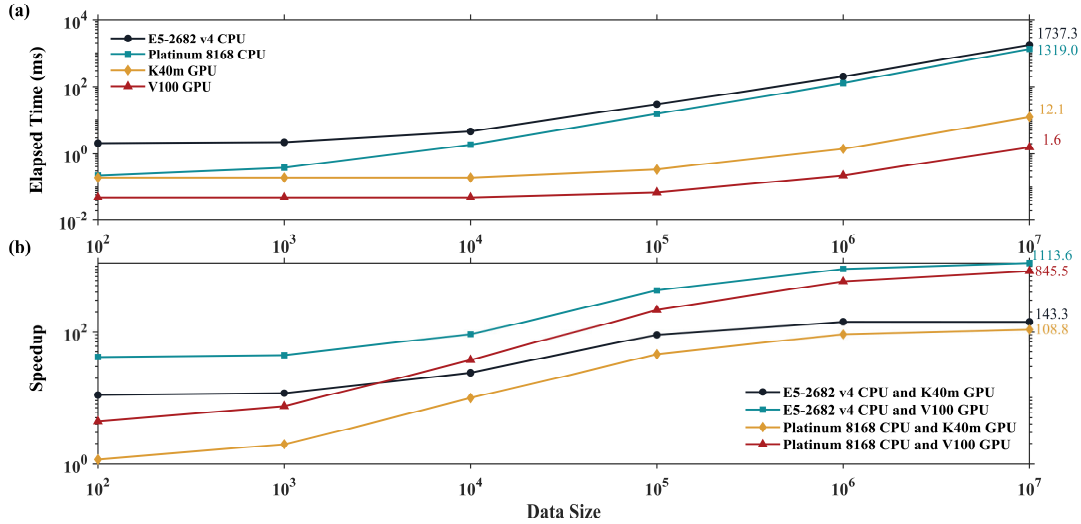
489 **Figure 9.** The offline performance of the HADVPPM and GPU-HADVPPM scheme on the CPU

490 and GPU. The unit of the wall times for the offline performance experiments is in milliseconds (ms).

491 **4.4. Coupling performance comparison of GPU-HADVPPM with different GPU**

492 **configurations**

493 **4.4.1. CAMx-CUDA on a single GPU**

494 The offline performance results show that the larger the data size is, the more

495 obvious the acceleration effect of the GPU-HADVPPM scheme. After coupling the

496 GPU-HADVPPM to CAMx without changing the advection module algorithm, the

497 overall computational efficiency of the CAMx-CUDA model is extremely low, and it

498 takes approximately 621 minutes to complete a one-hour integration on the V100

499 cluster. Therefore, according to the optimization scheme in Sect. 3.2, by optimizing the

500 algorithm of the xyadvec Fortran program, we gradually increase the size of the data

501 transmitted and reduce the data transmission frequency between the CPU and GPU.

502 When the data transmission frequency between the CPU and GPU is reduced to 1 within

503 one time step, we further optimize the GPU memory access order on the GPU card,

504 eliminate unnecessary assignment loops before kernel functions are launched and use

505   the thread and block indices.

506   Table 4 lists the total elapsed time for different versions of the CAMx-CUDA

507   model during the optimization, as described in Section 3.2. Since the xyadvec program

508   in CAMx-CUDA V1.0 is not optimized, it is extremely computationally inefficient

509   when starting two CPU processes and configuring a GPU card for P1. On the K40m

510   and V100 clusters, it takes 10829 seconds and 37237 seconds, respectively, to complete

511   a 1-hour simulation.

512   By optimizing the algorithm of the xyadvec Fortran program and hadvppm_kernel

513   CUDA C program, the data transmission frequency between the CPU and GPU was

514   decreased, and the overall computing efficiency was improved after GPU-HADVPPM

515   was coupled to the CAMx-CUDA model. In CAMx-CUDA V1.2, the data transmission

516   frequency between CPU-GPU within one time step is reduced to 1, the elapsed time on

517   the two heterogeneous clusters is 1207 seconds and 548 seconds, respectively, and the

518   speedup is 9.0x and 68.0x compared to CAMx-CUDA V1.0.

519   The GPU memory access order can directly affect the overall GPU-HAVPPM

520   computational efficiency on the GPU. In CAMx-CUDA V1.3, we optimized the

521   memory access order of the hadvppm_kernel CUDA C program on the GPU and

522   eliminated the unnecessary assignment loops before the kernel functions were launched,

523   which further improved the CAMx-CUDA model's computational efficiency, resulting

524   in 12.7x and 94.8x speedups.

525   Using thread and block indices to simultaneously compute the horizontal grid

526   points can greatly improve the computational efficiency of the GPU-HADVPPM and

527   thus reduce the overall elapsed time of the CAMx-CUDA model. CAMx-CUDA V1.4

528   further reduces the elapsed time by 378 seconds and 103 seconds on the K40m cluster

529   and V100 cluster, respectively, compared with CAMx-CUDA V1.3 and achieves up to

530   a 29.0x and 128.4x speedup compared with CAMx-CUDA V1.0.

531   **Table 4.** Total elapsed time for different versions of CAMx-CUDA during the optimization. The

532   unit of elapsed time for experiments is in seconds (s).

Versions	K40m cluster	V100 cluster

	Elapsed Time	Speedup	Elapsed Time	Speedup
CAMx-CUDA V1.0	10829	1.0	37237	1.0
CAMx-CUDA V1.1	1403	7.7	1082	34.4
CAMx-CUDA V1.2	1207	9.0	548	68.0
CAMx-CUDA V1.3	751	12.7	393	94.8
CAMx-CUDA V1.4	373	29.0	290	128.4

In terms of the single module computational efficiency of HADVPPM and GPU-HADVPPM, we further tested the computational performance of the Fortran version of HADVPPM on the CPU, C version of HADVPPM on the CPU, and the CUDA C version of GPU-HADVPPM in CAMx-CUDA V1.4 (GPU-HADVPPM V1.4) on the GPU using system_clock functions in the Fortran language and cudaEvent_t in CUDA programming. The specific results are shown in Figure 10. On the K40m cluster, it takes 37.7 seconds and 51.4 seconds to launch the Intel Xeon E5-2682 v4 CPU to run the Fortran and C version HADVPPM, respectively, and the C version is 26.7% slower than the Fortran version. After the CUDA technology was used to convert the C code into CUDA C, the CUDA C version took 29.6 seconds to launch an NVIDIA Telsa K40m GPU to run GPU-HADVPPM V1.4, with a 1.3x and 1.7x acceleration. On the V100 cluster, the Fortran, C, and CUDA C versions are computationally more efficient than those on the K40m cluster. It takes 30.1 seconds and 45.2 seconds to launch the Intel Xeon Platinum 8168 CPU to run the Fortran and C version HADVPPM, and 1.6 seconds to run the GPU-HADVPPM V1.4 using an NVIDIA V100 GPU. The computational efficiency of the CUDA C version is 18.8x and 28.3x higher than the Fortran and C versions, respectively.
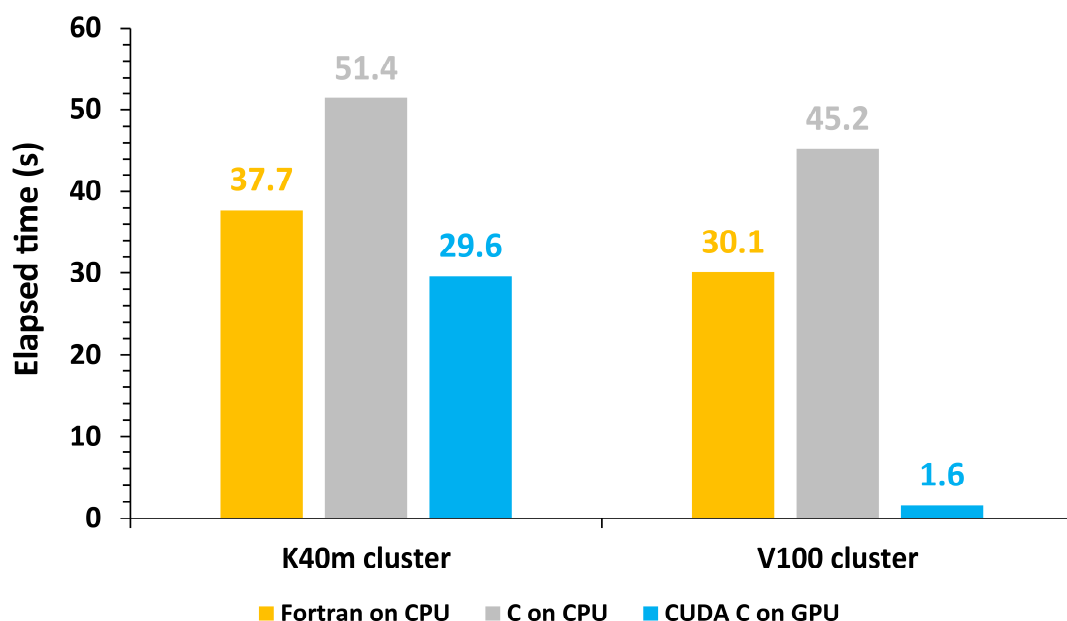
Figure 10. The elapsed time of the Fortran version HADVPPM on the CPU, the C version HADVPPM on the CPU and the CUDA C version GPU-HADVPPM V1.4 on the GPU. The unit is in seconds (s).

4.4.2. CAMx-CUDA on multiple GPUs

To make full use of the multicore and multi-GPUs in the heterogeneous cluster, the MPI+CUDA acceleration algorithm was implemented to improve the total computational performance of the CAMx-CUDA model. Two different compile flags were implemented in this study before comparing the computational efficiency of CAMx-CUDA V1.3 and V1.4 on multiple GPUs, namely, *-mieee-fp* and *-fp-model precise*. The *-mieee-fp* compile flag comes from the *Makefile* of the official CAMx version, which uses the IEEE standard to compare the floating-point numbers. Its computational accuracy is higher but the efficiency is slower. The *-fp-model precise* compile flag controls the balance between the precision and efficiency of the floating-point calculations, and it can force the compiler to use the vectorization of some calculations under value safety. The experimental results show that the *-fp model precise* compile flag is 41.4% faster than *-mieee-fp*, and the AEs of the simulation results are less than ± 0.05 ppbv (Figure S3). Therefore, the *-fp model precise* compile flag is implemented when comparing the computational efficiency of CAMx-CUDA

569 V1.3 and V1.4 on multiple GPU cards. Figure 11 shows the total elapsed time and

570 speedup of CAMx-CUDA V1.3 and V1.4 on the V100 cluster. The total elapsed time

571 decreases as the number of CPU cores and GPU cards increases. When starting 8 CPU

572 cores and 8 GPU cards, the speedup of CAMx-CUDA V1.4 is increased from 3.9x to

573 4.5x compared with V1.3, and the computational efficiency is increased by 35.0%.
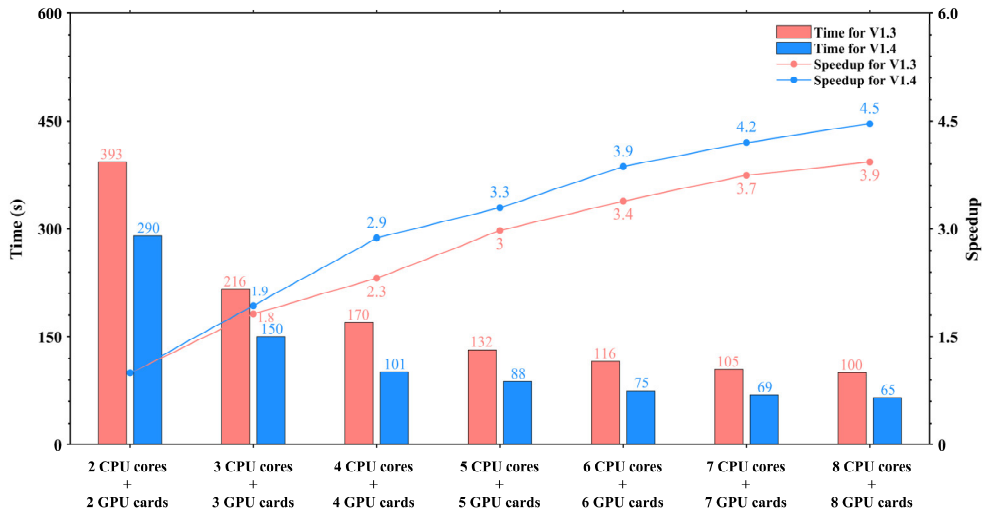
574

575 **Figure 11.** The total elapsed time and speedup of CAMx-CUDA V1.3 and V1.4 on multiple

576 GPUs. The unit of elapsed time for experiments is seconds (s).

577 **5. Conclusions and discussion**

578   GPU accelerators are playing an increasingly important role in high-performance

579 computing. In this study, a GPU acceleration version of the PPM solver (GPU-

580 HADVPPM) of horizontal advection for an air quality model was developed, which

581 runs on GPU accelerators using the standard C programming language and CUDA

582 technology. The offline performance experimental results showed that the K40m and

583 V100 GPU can achieve up to a 845.4x and 1113.6x speedup, respectively, and the larger

584 the data input to the GPU, the more obvious the acceleration effect. After coupling the

585 GPU-HADVPPM to the CAMx model, a series of optimization measures were taken,

586 including reducing the CPU-GPU communication frequency, increasing the data

computation size on the GPU, optimizing the GPU memory access order and using thread and block indices to improve the overall computing performance of the CAMx-CUDA model. Using a single GPU card, the optimized CAMx-CUDA V1.4 model improved the computing efficiency by 29.0x and 128.4x on the K40m cluster and the V100 cluster, respectively. In terms of the single-module computational efficiency of GPU-HADVPPM, it achieved a 1.3x and 18.8x speedup on an NVIDIA Tesla K40m GPU and NVIDA Tesla V100 GPU, respectively. To make full use of the multicore and multi-GPU supercomputers and further improve the total computational performance of the CAMx-CUDA model, a parallel architecture with an MPI+CUDA hybrid paradigm was presented. After implementing the acceleration algorithm, the total elapsed time decreased as the number of CPU cores and GPU cards increased, and it achieved up to a 4.5x speedup when launching 8 CPU cores and 8 GPU cards compared with 2 CPU cores and 2 GPU cards.

However, the current approach has some limitations, which are as follows:

1) We currently implement thread and block coindexing to compute horizontal grid points in parallel. Given the CAMx Model 3-dimensional grid computing characteristics, in the future, 3-dimensional thread and block coindexing will be considered to compute 3-dimensional grid points in parallel.

2) The communication bandwidth of data transfer is one of the main issues restricting the computing performance of the CUDA C codes on the GPUs. This restriction holds true not only for GPU-HADVPPM but also for the WRF module (Mielikainen et al., 2012b; Mielikainen et al., 2013b; Huang et al., 2013). In this study, the data transmission efficiency between the CPU and GPU is improved only by reducing the communication frequency. In the future, more technologies, such as pinned memory (Wang et al., 2016), will be considered to resolve the communication bottleneck between the CPUs and GPUs.

3) To further improve the overall computational efficiency of the CAMx model, the heterogeneous porting scheme proposed in this study will be considered to conduct the heterogeneous porting of other CAMx modules in the future.

Code and data availability. The source codes of CAMx version 6.10 are available at https://camx-wp.azurewebsites.net/download/source/(last access: 24 March 2023, ENVIRON,2022). The dataset related to this paper and the CAMx-CUDA codes are available online via ZENODO (http://doi.org/10.5281/zenodo.7765218; Cao et al.,2023).

Author contributions. KC conducted the simulation and prepared the materials. QZW, LLW and LNW planned and organized the project. KC, QZW and XT refactored and optimized the codes. LLW, NW, HQC and DQL collected and prepared the data for the simulation. KC, QZW, XT and LNW participated in the discussion.

Competing interests. The authors declare that they have no conflicts of interest.

Acknowledgements. The National Key R&D Program of China (2020YFA0607804 & 2017YFC0209805), the National Supercomputing Center in Zhengzhou Innovation Ecosystem Construction Technology Special Program (Grant No. 201400210700) and the Beijing Advanced Innovation Program for Land Surface funded this work. The research is supported by the High Performance Scientific Computing Center (HSCC) of Beijing Normal University and the National Supercomputing Center in Zhengzhou.

References

Bleichrodt, F., Bisseling, R. H., and Dijkstra, H. A.: Accelerating a barotropic ocean model using a GPU, Ocean Modelling, 41, 16-21, 10.1016/j.ocemod.2011.10.001, 2012.

Cao, K., Wu, Q., Wang, L., Wang, N., Cheng, H., Tang, X., Li, D., and Wang, L.: The dataset of the manuscript "GPU-HADVPPM V1.0: high-efficient parallel GPU

design of the Piecewise Parabolic Method (PPM) for horizontal advection in air quality model (CAMx V6.10)", ZENODO, https://doi.org/10.5281/zenodo.7765218, 2023.

Colella, P. and Woodward, P. R.: The Piecewise Parabolic Method (PPM) for gas-dynamical simulations, Journal of Computational Physics, 54, 174-201, https://doi.org/10.1016/0021-9991(84)90143-8, 1984.

ENVIRON: User Guide for Comprehensive Air Quality Model with Extensions Version 6.1, available at: https://camx-wp.azurewebsites.net/Files/CAMxUsersGuide_v6.10.pdf (last access: 19 December 2022), 2014

Govett, M., Rosinski, J., Middlecoff, J., Henderson, T., Lee, J., MacDonald, A., Wang, N., Madden, P., Schramm, J., and Duarte, A.: Parallelization and Performance of the NIM Weather Model on CPU, GPU, and MIC Processors, Bulletin of the American Meteorological Society, 98, 2201-2213, 10.1175/bams-d-15-00278.1, 2017.

Houyoux, M. R. and Vukovich, J. M.: Updates to the Sparse Matrix Operator Kernel Emissions (SMOKE) Modeling System and Integration with Models-3,

Huang, B., Mielikainen, J., Plaza, A. J., Huang, B., Huang, A. H. L., and Goldberg, M. D.: GPU acceleration of WRF WSM5 microphysics, High-Performance Computing in Remote Sensing, 10.1117/12.901826, 2011.

Huang, B., Huang, M., Mielikainen, J., Huang, B., Huang, H. L. A., Goldberg, M. D., and Plaza, A. J.: On the acceleration of Eta Ferrier Cloud Microphysics Scheme in the Weather Research and Forecasting (WRF) model using a GPU, High-Performance Computing in Remote Sensing II, 10.1117/12.976908, 2012.

Huang, M., Huang, B., Chang, Y.-L., Mielikainen, J., Huang, H.-L. A., and Goldberg, M. D.: Efficient Parallel GPU Design on WRF Five-Layer Thermal Diffusion Scheme, IEEE Journal of Selected Topics in Applied Earth Observations and Remote Sensing, 8, 2249-2259, 10.1109/jstars.2015.2422268, 2015.

Huang, M., Huang, B., Mielikainen, J., Huang, H. L. A., Goldberg, M. D., and Mehta, A.: Further Improvement on GPU-Based Parallel Implementation of WRF 5-Layer

Thermal Diffusion Scheme, 2013 International Conference on Parallel and Distributed Systems, 10.1109/icpads.2013.126, 2013.

Jiang, J., Lin, P., Wang, J., Liu, H., Chi, X., Hao, H., Wang, Y., Wang, W., and Zhang, L.: Porting LASG/ IAP Climate System Ocean Model to Gpus Using OpenAcc, IEEE Access, 7, 154490-154501, 10.1109/access.2019.2932443, 2019.

Mielikainen, J., Huang, B., Huang, H.-L. A., and Goldberg, M. D.: GPU Acceleration of the Updated Goddard Shortwave Radiation Scheme in the Weather Research and Forecasting (WRF) Model, IEEE Journal of Selected Topics in Applied Earth Observations and Remote Sensing, 5, 555-562, 10.1109/jstars.2012.2186119, 2012a.

Mielikainen, J., Huang, B., Huang, H.-L. A., and Goldberg, M. D.: GPU Implementation of Stony Brook University 5-Class Cloud Microphysics Scheme in the WRF, IEEE Journal of Selected Topics in Applied Earth Observations and Remote Sensing, 5, 625-633, 10.1109/jstars.2011.2175707, 2012b.

Mielikainen, J., Huang, B., Huang, H. L. A., Goldberg, M. D., and Mehta, A.: Speeding Up the Computation of WRF Double-Moment 6-Class Microphysics Scheme with GPU, Journal of Atmospheric and Oceanic Technology, 30, 2896-2906, 10.1175/jtech-d-12-00218.1, 2013a.

Mielikainen, J., Huang, B., Wang, J., Allen Huang, H. L., and Goldberg, M. D.: Compute unified device architecture (CUDA)-based parallelization of WRF Kessler cloud microphysics scheme, Computers & Geosciences, 52, 292-299, 10.1016/j.cageo.2012.10.006, 2013b.

NVIDIA: CUDA C++ Programming Guide Version 10.2, available at: https://docs.nvidia.com/cuda/archive/10.2/pdf/CUDA_C_Programming_Guide.pdf (last access: 19 December 2022), 2020

NVIDIA: Floating Point and IEEE 754 Compliance for NVIDIA GPUs. Release 12.1, available at: https://docs.nvidia.com/cuda/floating-point/#differences-from-x86 (last access: 18 May 2023), 2023.

Odman, M. and Ingram, C.: Multiscale Air Quality Simulation Platform (MAQSIP):

Source Code Documentation and Validation, 1996.

Price, E., Mielikainen, J., Huang, M., Huang, B., Huang, H.-L. A., and Lee, T.: GPU-Accelerated Longwave Radiation Scheme of the Rapid Radiative Transfer Model for General Circulation Models (RRTMG), IEEE Journal of Selected Topics in Applied Earth Observations and Remote Sensing, 7, 3660-3667, 10.1109/jstars.2014.2315771, 2014.

Skamarock, W. C., Klemp, J. B., Dudhia, J., Gill, D. O., Barker, D.M., Duda, M. G., Huang, X. Y., Wang, W., and Powers, J. G.: A Description of the Advanced Research WRF Version3 (No.NCAR/TN-475CSTR), University Corporation for Atmospheric Research, https://doi.org/10.5065/D68S4MVH, NCAR, 2008.

Streets, D. G., Zhang, Q., Wang, L., He, K., Hao, J., Wu, Y., Tang, Y., and Carmichael, G. R.: Revisiting China's CO emissions after the Transport and Chemical Evolution over the Pacific (TRACE-P) mission: Synthesis of inventories, atmospheric modeling, and observations, Journal of Geophysical Research: Atmospheres, 111, https://doi.org/10.1029/2006JD007118, 2006.

Streets, D. G., Bond, T. C., Carmichael, G. R., Fernandes, S. D., Fu, Q., He, D., Klimont, Z., Nelson, S. M., Tsai, N. Y., Wang, M. Q., Woo, J. H., and Yarber, K. F.: An inventory of gaseous and primary aerosol emissions in Asia in the year 2000, Journal of Geophysical Research: Atmospheres, 108, https://doi.org/10.1029/2002JD003093, 2003.

Sun, Y., Wu, Q., Wang, L., Zhang, B., Yan, P., Wang, L., Cheng, H., Lv, M., Wang, N., and Ma, S.: Weather Reduced the Annual Heavy Pollution Days after 2016 in Beijing, Sola, 18, 135-139, 10.2151/sola.2022-022, 2022.

Wahib, M. and Maruyama, N.: Highly optimized full GPU-acceleration of non-hydrostatic weather model SCALE-LES, 2013 IEEE International Conference on Cluster Computing (CLUSTER), 23-27 Sept. 2013, 1-8, 10.1109/CLUSTER.2013.6702667,

Wang, P., Jiang, J., Lin, P., Ding, M., Wei, J., Zhang, F., Zhao, L., Li, Y., Yu, Z., Zheng, W., Yu, Y., Chi, X., and Liu, H.: The GPU version of LASG/IAP Climate System

Ocean Model version 3 (LICOM3) under the heterogeneous-compute interface for portability (HIP) framework and its large-scale application, Geosci. Model Dev., 14, 2781-2799, 10.5194/gmd-14-2781-2021, 2021a.

Wang, Y., Guo, M., Zhao, Y., and Jiang, J.: GPUs-RRTMG_LW: high-efficient and scalable computing for a longwave radiative transfer model on multiple GPUs, The Journal of Supercomputing, 77, 4698-4717, 10.1007/s11227-020-03451-3, 2021b.

Wang, Z., Wang, Y., Wang, X., Li, F., Zhou, C., Hu, H., and Jiang, J.: GPU-RRTMG_SW: Accelerating a Shortwave Radiative Transfer Scheme on GPU, IEEE Access, 9, 84231-84240, 10.1109/access.2021.3087507, 2016.

Xiao, H., Lu, Y., Huang, J., and Xue, W.: An MPI+OpenACC-based PRM scalar advection scheme in the GRAPES model over a cluster with multiple CPUs and GPUs, Tsinghua Science and Technology, 27, 164-173, 10.26599/TST.2020.9010026, 2022.

Xu, S., Huang, X., Oey, L. Y., Xu, F., Fu, H., Zhang, Y., and Yang, G.: POM.gpu-v1.0: a GPU-based Princeton Ocean Model, Geoscientific Model Development, 8, 2815-2827, 10.5194/gmd-8-2815-2015, 2015.

Zhang, Q., Streets, D. G., Carmichael, G. R., He, K. B., Huo, H., Kannari, A., Klimont, Z., Park, I. S., Reddy, S., Fu, J. S., Chen, D., Duan, L., Lei, Y., Wang, L. T., and Yao, Z. L.: Asian emissions in 2006 for the NASA INTEX-B mission, Atmos. Chem. Phys., 9, 5131-5153, 10.5194/acp-9-5131-2009, 2009.